# The Report
# on
# Summer Project 2019

**Worked At**

# Deutsches Elektronen Synchrotron (DESY)

**on**

## Experimental and Theoretical Investigation of Photofrgamentation Mechanisms of Polycyclic Aromatic Hydrocarbons (PAHs) Exposed to XUV Radiation


Presented by

**Amlan Datta**

$3^{rd}$ Year, 16MS156

Department of Physical Sciences

Indian Institute of Science Education and Research (IISER) Kolkata




*Under guidance of:*

**Prof. Dr. Melanie Schnell**

Deutsches Elektronen Synchrotron DESY, Hamburg, Germany

# *Acknowledgements*

I am deeply indebted to my project supervisor Prof. Dr. Melanie Schnell, FS-SMP(Photon Science- Spectroscopy of Molecular Processes), Deutsches Elektronen Synchrotron DESY, Hamburg, Germany for her all-out support, valuable advice, and encouragement.

I am specially grateful to Dr. Denis Tikhonov, FS-SMP, Deutsches Elektronen Synchrotron DESY, Hamburg, Germany, for his entire help, advices and encouragement throughout the project.

I convey thanks to Dr. Donatella Loru, FS-SMP, Deutsches Elektronen Synchrotron DESY, Hamburg, Germany for providing me an interactive experimental environment.

I am also grateful to Prgya Chopra and other members of FS-SMP, Deutsches Elektronen Synchrotron DESY, Hamburg, Germany and all of my teachers of my institute, Indian Institute of Science Education and Research, Kolkata, for their all the round moral support.

I must mention my parents Prof. Utpal Datta and Mrs. Rajashree Datta for their valuable advice and support, which I receive all the time.

I am also grateful to Deutsches Elektronen Synchrotron DESY, Hamburg, Germany for sponsoring my visit. I would like to extend my deep gratitude to the Ministry of Human Resource Development, Govt. of India, and Department of Science & Technology, Govt. of India for the highly expected encouragement for participating in the project.

**Amlan Datta**

$3^{rd}$ Year, 16MS156

Indian Institute of Science Education and Research (IISER) Kolkata

Date: $15^{th}$ July, 2019

*"Being kind to yourself is one of the greatest kindness."*

*....said the mole.*

# Contents

# List of Figures

**Page**

**Abstract**

The study of molecular dynamics involves the observations and analysis of electronic and nuclear motions. Nuclear motions happen on picosecond and femtosecond timescale, and electronic motions appear at attosecond timescale. Ultrashort laser pulses are used as an essesntial tool for triggering and probing the femtosecond dynamcs by interaction with the target molecule. This allows us to take snapshots and look at the motions on the timescales, comparable with the laser pulses duration. In this work we have analyzed experimental data obtained at free electron laser in Hamburg (FLASH), that produces pulses with XUV photon energy.

The first part of the report contains the analysis of the partial covariance maps of three PAHs of our interest: Fluorene, Phenanthrene and Pyrene. This is an investigation of mechanisms behind photofragmentation of these molecules subjected to harsh XUV radiation. The idea for that is to simulate the processes appearing in the interstellar medium (ISM), when the PAHs are excited by spaceous syncrotron radiation sources (such as Crab Nebula, etc.). The results from the time-of-flight – time-of-flight (TOF-TOF) partial covariance maps of these molecules are presented and analyzed to observe their behaviour under XUV excitation.

The second part is theoretical modeling of the photochemical dynamics. It is inspired from the experimental results of some ultrafast pump-probe dynamics research going on all over the world including the study depicted in the first part of the report. Simulations are very nice tool in science to analyze the phenomena happening in the labs. So, in addition to pure experiment, simulation methods are implemented to see whether they match with the experimental data. We have focussed on the single photon excitation processes only and we have taken the reference accordingly. Most importantly we are concerned more about the nuclear dynamics which leads to better understanding of fragmentations in pump-probe experiments. Also the result or more specifically the pump-probe fragmentation dynamics

yields from the simulations will lead us better understanding of the physics of these processes in pump-probe experiments.

# Chapter 1

# Investigation of Photofragmentation Mechanisms of PAHs using Covariance Mappping Analysis

# Introduction

According to Born–Oppenheimer approximation, internal molecular motions can be separated into nuclear and electronic dynamics. But they are not necessarily independent of each other. After electronic excitation caused by the absprption of the photon, the equilibrium of the nuclear potential is shifted and this gives rise to the vibrational excitations. Now if this excitation exceeds the dissociation energy then the photodissociation can occur. The change in nuclear positions is effectively a change in bond length. This can lead to bond breaking and dissociation processes followed by fragmentation into charged and neutral fragments. The photoion-photoion correlations in the molecule is studied via covariance mapping technique.[3, 7]

## 1.1 Covariance mapping

### 1.1.1 General introduction to covariance and application to our investigation

In probability and statistics, covariance is a measure of the relationship between two random variables. The metric evaluates how much i.e. to what extent the variables change together. Let us assume two random variables $X$ and $Y$. The covariance of these two variables is a measure of the joint variability. In general the covariance is calculated as,

$$\begin{aligned} \mathrm{cov}(X,Y) = \langle (X - \langle X\rangle)\cdot(Y - \langle Y\rangle)\rangle = \langle XY\rangle - \langle X\rangle\langle Y\rangle \\ \text{where } \langle X\rangle = \frac{1}{N}\sum_{n=1}^{N} X_n \text{ and } \langle XY\rangle = \frac{1}{N}\sum_{n=1}^{N} X_n Y_n \end{aligned} \tag{1.1}$$

And self-covarinace i.e the diagonal matrix of diagonal elements of the covariance matrix is the standard deviation of the joint distribution.

$$\begin{aligned} \mathrm{cov}(X,X) = \langle X^2\rangle - \langle X\rangle^2 = \sigma_X^2 \\ \mathrm{cov}(Y,Y) = \langle Y^2\rangle - \langle Y\rangle^2 = \sigma_Y^2 \end{aligned}$$

If the greater values of one variable mainly correspond with the greater values of the other variable, and the same holds for the lesser values, (i.e., the variables tend to show similar behavior), the covariance is positive. In the opposite case, when the greater values of one variable mainly correspond to the lesser values of the other, (i.e., the variables tend to show opposite behavior), the covariance is negative. The sign of the covariance therefore shows the tendency of the linear relationship between the variables.

We are interested in the Time of Flight (TOF) correlation maps where we have TOF-MS (TOF Mass Spectra) as an array of "Time vs. Ion intensity" $I_i^{\mathrm{TOF}} = I^{\mathrm{TOF}}(t_i)$, with a length of $M$(say) elements. TOF-MS is measured at each shot of lasers providing $N$ independent measurements, i.e. for each TOF-MS point $I_i^{\mathrm{TOF}} = I^{\mathrm{TOF}}(t_i)$ we have $N$ independent measurements as $\left\{I_{in}^{\mathrm{TOF}}\right\}_{n=1}^{N}$. So in principle we can now construct an $M \times M$ covariance matrix whose elemnets are given by the following,

$$C_{ij} = \mathrm{cov}(I_i^{\mathrm{TOF}}, I_j^{\mathrm{TOF}}) = \frac{1}{N}\sum_{n=1}^{N} I_{in}^{\mathrm{TOF}} I_{jn}^{\mathrm{TOF}} - \left(\frac{1}{N}\sum_{n=1}^{N} I_{in}^{\mathrm{TOF}}\right) \cdot \left(\frac{1}{N}\sum_{n=1}^{N} I_{in}^{\mathrm{TOF}}\right) \tag{1.2}$$

As already mentioned above, we now need to consider the sign of covariance to see how they behave.

- If increase in intesity in one point also increases the intensity in the other point accordingly then the sign will be positive i.e cov $> 0$.
- If increase in intesity in one point decreases the intensity in the other point then the sign will be negative i.e cov $< 0$.
- If the intensity at two points change independently then the covariance is zero.

However, in the experiments can be a third strond random variable (Z), that correlates every signal with every signal. In our case it is the energy of XUV pulse produced by the FEL. It fluctuates greatly, and at the same time its intencity is proportional to the number of molecules ionized. Therefore the influence of this random variable should be eliminated. It can be done using so-called partial covariance matrixes.[4, 12] So structure of the partial covariance looks like,

$$\mathrm{pcov}(X, Y) = \mathrm{cov}(X, Y) - \frac{\mathrm{cov}(X, Z) \cdot \mathrm{cov}(Y, Z)}{\sigma_Z^2}$$

where $Z$ is the third correlated random variable. The elements of the partial covariance matrix of the TOF-TOF mass spectra accounting for FEL intensity $I^{\mathrm{FEL}}$ fluctuation are,

$$P_{ij} = C_{ij} - \frac{\mathrm{cov}(I_i^{\mathrm{TOF}}, I^{\mathrm{FEL}}) \cdot \mathrm{cov}(I_j^{\mathrm{TOF}}, I^{\mathrm{FEL}})}{\sigma^2_{I^{\mathrm{FEL}}}} \tag{1.3}$$

where,

$$\mathrm{cov}(I_k^{\mathrm{TOF}}, I^{\mathrm{FEL}}) = \frac{1}{N}\sum_{n=1}^{N} I_{kn}^{\mathrm{TOF}} I_n^{\mathrm{FEL}} - \left(\frac{1}{N}\sum_{n=1}^{N} I_{kn}^{\mathrm{TOF}}\right) \cdot \left(\frac{1}{N}\sum_{n=1}^{N} I_n^{\mathrm{FEL}}\right)$$

### 1.1.2 Mechanism of Coulomb explosion and partial covariance map analysis

Coulomb explosions are a sort of photofragmentation reactions that look in general as $\mathrm{AB}^{n+} \rightarrow \mathrm{A}^{q+} + \mathrm{B}^{(n-q)+}$, where $n$, $q$ and $n-q$ are greater than 0 (see Fig. 1.1.1 for illustration).[3]

These types of reactions appear as a very specific features in the TOF-TOF covariance maps.

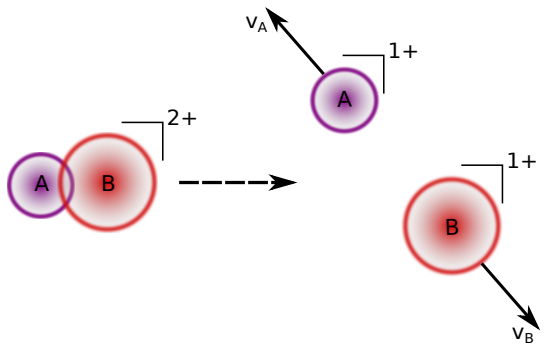


Figure 1.1.1: The figure shows the scheme of the process known as Coulomb explosion where two ions of same sign of charge drift apart from each other due to high interionic Coulomb repulsion.

Let us assume that we have a dication $\mathrm{AB}^{2+}$ which decays as follows,

$$\mathrm{AB}^{2+} \longrightarrow \mathrm{A}^{+} + \mathrm{B}^{+}$$

The intensities of the ion fragments $A^+$ and $B^+$ will correlate with cov $> 0$ as they are formed from the same dication and the overall kinetic energy of the dication is shared between the two fragments. But they will not reach the detector at same time and this is the catch!

Due to intra-ionic repulsions as they have same sign of charge, will drift apart from each

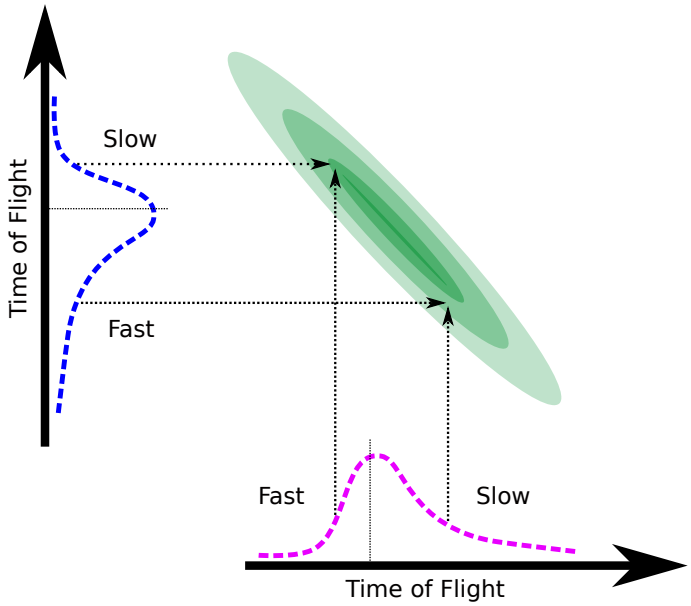


Figure 1.1.2: This figure shows the scheme of formation of the slope in Coulomb explosion on the covariance maps.

other as shown in Fig. 1.1.1. The electric field applied to detect the particles acts as an external force field for the whole system and the centre of mass will keep moving along the same direction as it was before. Only due to internal forces i.e. the inter-ionic repulsion the fragment ions will get separated and hit the detector at different times. So based on that, if one ion is fast in the direction of detector then the other part is slow and vice versa. Hence the slope we will have is equal to -1 as in shown in Fig. 1.1.2 in the covariance map for cov $< 0$.

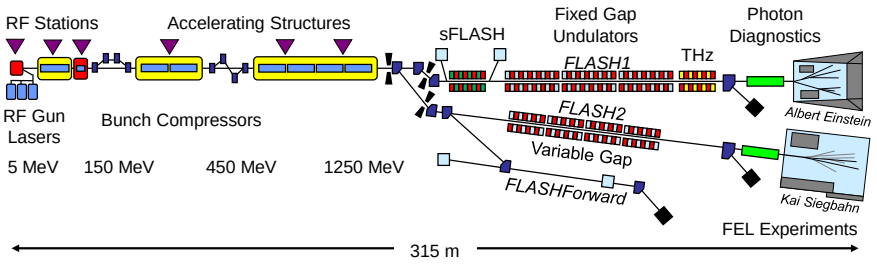


Figure 1.2.1: Schematic diagram of the FLASH (`https://flash.desy.de/`)

## 1.2 Experimental Setup at FLASH

In the Fig. 1.2.1, the entire setup of FLASH is shown. here are two experimental halls at FLASH and each of them has several endstations. We have worked with the data from CAMP(an end station at Albert Einstein hall as in Fig. 1.2.1), a multi-Purpose end-station for Electron- and Ion-Spectroscopy, Pump-Probe, and Imaging Experiments at FLASH[1] end station as shown in Fig. 1.2.3 which is at FLASH 1. At CAMP the main process done via VMI.

Measuring the energy- and spatial distribution of photoelectrons makes it possible to in-

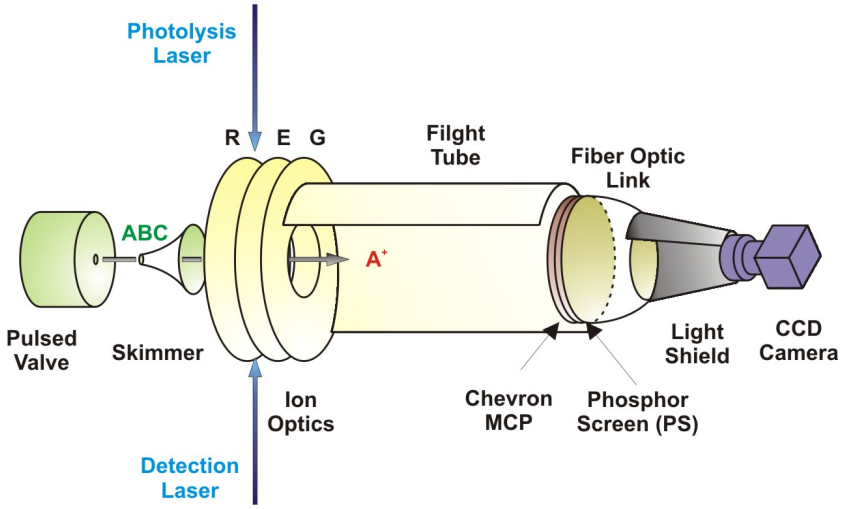


Figure 1.2.2: The general structure of VMI setup (`https://en.wikipedia.org/wiki/Photofragment-ion_imaging`).

[1]FLASH- the Free-Electron LASer in Hamburg, Deutsches Elektronen-Synchrotron DESY, Germany

vestigate the internal electronic structure of the atoms and molecules. The easiest way is to measure the time of flight of the ions to a detector that is placed at different positions with respect to the ionizing laser field. But it takes long measuring times. Velocity map imaging (VMI) is a technique which makes it possible to cover the whole solid angle in one measurement and to measure the energies and emission angles of all ions and photoelectrons at once. For this the photoelectrons and ions are imaged onto a position sensitive detector using an electrostatic lens created by inhomogeneous electrical fields. Velocity map imaging is based on the use of an electrostatic lens to accelerate the ions toward the detector. When the voltages are properly adjusted, this lens has the advantage that it focuses ions with the same velocity to a single spot on the detector irrespective of the positions where the ions were created where the ion was created. From the Fig. 1.2.2, we get an idea how the system works. Just after supersonic expansion the ions and the photoelectrons are guided by the electrostatic lenses. There are three layes of lens arrangement and those are, **R**: Repeller, **E**: Extractor and **G**: Ground. Now the fragment ions or the photoelectrons travel a distance through the flight tube and they reach the Chevron MCP (MCP stands for Micro-channel plate) and at the end of it there is the phospher screen (PS). The phospher screen is attached to the fibre optic link which is connected to the CCD (Charge-coupled device) camera. So we can see from Fig. 1.2.3, there is a single-photon counting pnCCD photon-detectors attached to the VMI setup. It is possible to mount PImMS etc. also.

The electrons and ions produced by photoionization and photodissociation are detected by static or electric or magnetic field in order to accelerate towards a detector (In our experiemnet we have used electric field for acceleration). This allows the discriminations of the ions based on mass-to-charge ratio ($m/q$) and the initial kinetic energy. The spectral information obtained through these aproaches allows the resolution of the very fine structures, such as vibrational electronic states in molecules, and allows the analysis of correlation between the recorded channels, which provides us the informations about the processes such as **Coulomb explosions** or hydrogen transfer. As shown in the Fig. 1.2.4, we have the FLASH pulse which is the pump XUV pulse and the 400nm probe pulse coming from the other direction, making some angle with the pump pulse. They both act on the target molecule and the electric field is applied perpendicular to the plane containing the laser pulses. There is the TOF

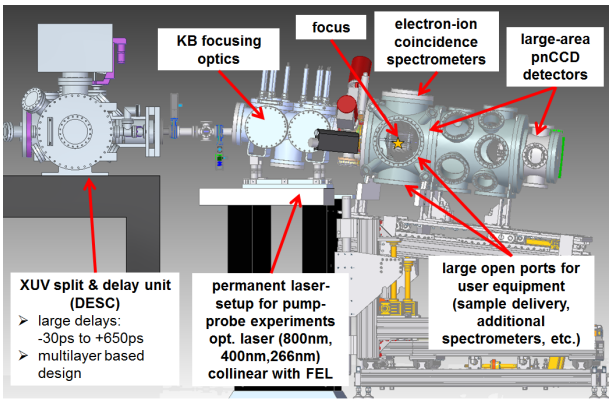


Figure 1.2.3: Schematic diagram of Camp end station at FLASH (`http://photon-science.desy.de/facilities/flash/beamlines/bl_beamlines_flash1/camp/index_eng.html`)

detector at end of the field where the particles are detected. The gas jet used for supersonic expansion was helium at temperature of 200 °C and 2 bar of pressure.

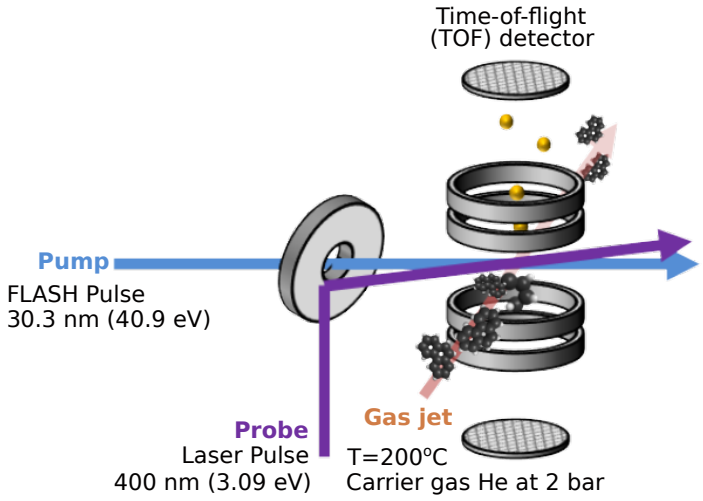


Figure 1.2.4: Schematic diagram of processes at CAMP end station

## 1.3 Analysis of partial covariance maps of molecules of interest

The molecules of interest for our purpose of experiment are phenanthrene($C_{14}H_{10}$), pyrene($C_{16}H_{10}$) and fluorene($C_{13}H_{10}$). We have used the data from CAMP to analyze and find Coulomb explosions. Based on data from March 2018 Bematime at FLASH, we have classified the data sets into two groups. The group 1 corresponds to all short range delay scans and with the photo diode scan switched on and group 2 conatins a mixture of data explained later.

### 1.3.1 Calibration

To interpret the covariance map we need to know the flight times of the fragments. As we have the TOF mass spectra of the molecule, we can calculate the TOF of each fragment. So, let us first look at the relation between $m/q$ and TOF. We have applied the static electric field $E_{\text{app}}$ to the ion formed by pump-probe application and the centre of mass gets accelerated and after Coulomb explosion the fragments start moving tomards the detector. The net force applied to the the particular ion fragment is equal to $q_{\text{ion}}E_{\text{app}}$. Let us assume that the length of the tube where we have applied the electric field i.e the length ions have to travel to reach the end of the field where we have the detector is $L$. So from Newton's equation of motion we have,

$$\begin{aligned} L &= \frac{1}{2}\left(\frac{q_{\text{ion}}E_{\text{app}}}{m_{\text{ion}}}\right)(t-t_0)^2 \\ \Rightarrow \frac{m_{\text{ion}}}{q_{\text{ion}}} &= \frac{E_{\text{app}}}{2\cdot L}(t-t_0)^2 \end{aligned} \tag{1.4}$$

where, $t$ is the time of flight of the ion and $t_0$ is the time when the Coulomb exolosion occurred. We don't know $L$, $E_{\text{app}}$ and $t_0$.

$$\boxed{\frac{m_{\text{ion}}}{q_{\text{ion}}} = K_{\text{ins}}\cdot(t-t_0)^2} \tag{1.5}$$

We have now a constant $K_{\text{ins}}$ which comes from the property of the experimetal apparatus and $t_0$ i.e two unknowns to solve the equation as we know $\frac{m_{\text{ion}}}{q_{\text{ion}}}$ for the parent ion ($PAH^+$) and the $He^+$. So after we get the value for the constant and the explosion time we can calculate

the TOF for all other fragments.

### 1.3.2 Group 1

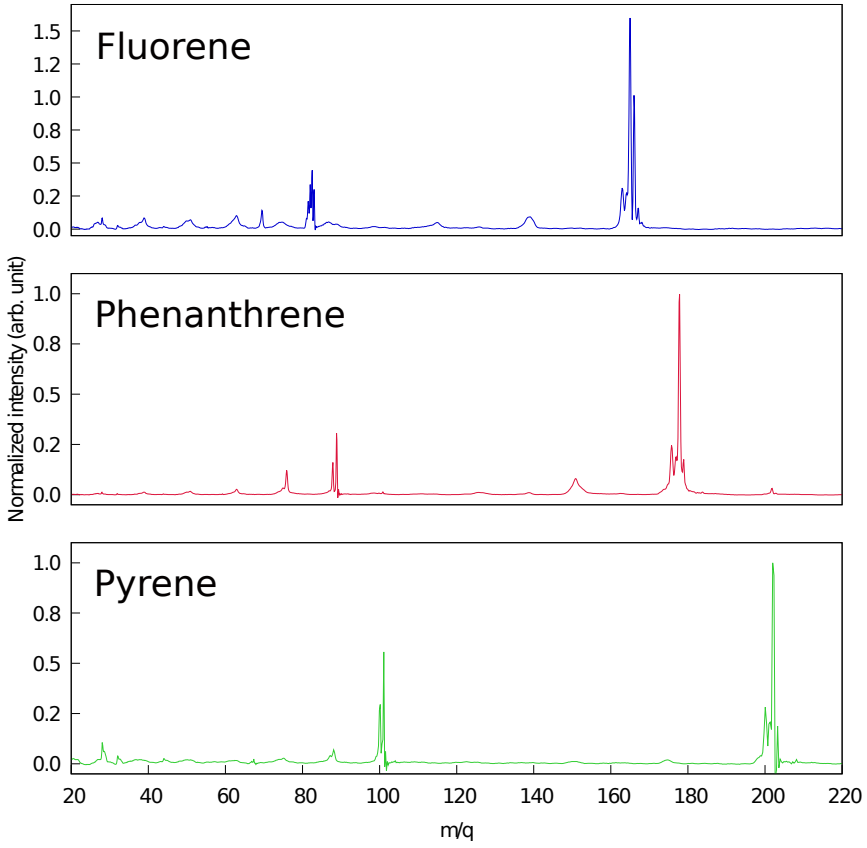


Figure 1.3.1: Time of flight Mass spectra of fluorene, phenanthrene and pyrene.

The experiemntal conditions for the Group 1 are:

1. FEL pump
2. 400 nm probe.
3. Delay scan is on.
4. Photo-diode scan is on.

In this group we have three PAHs (Polycylic Aromatic hydrocarbon) to work with,

1. Phenanthrene
2. Pyrene
3. Fluoerene.

#### 1.3.2.1 Fluorene

Molecular formula of fluorene: $C_{13}H_{10}$
Molar mass of fluorene:166 g/mol
2D structure of fluorene:

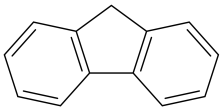

**Calibration for Flourene:**
From the TOF Mass spectra of fluorene in Fig. 1.3.1, We have,

$$\frac{m_{\mathrm{Flu}^+}}{q_{\mathrm{Flu}^+}} = 166,\ \frac{m_{\mathrm{He}^+}}{q_{\mathrm{He}^+}} = 4$$
$$t_{\mathrm{Flu}^+} = 2488,\ t_{\mathrm{He}^+} = 569$$
$$(\mathrm{Flu}:\ \mathrm{Fluorene},\ \mathrm{He}:\ \mathrm{Helium})$$

Plugging the values in eqn. 1.5 and solving for $K_{\mathrm{ins}}$ and $t_0$, we get,

$$\boxed{K_{\mathrm{ins}} = 3.2168 \times 10^{-5}, \text{and } \mathrm{t}_0 = 216.3754}$$

From the covarinace map we have plotted in Fig. 1.3.2, we see three lines corresponding to Coulomb explosions.

- $\mathbf{C_2}$ loss:
  Time of flight of first ion: 1150.01 ms
  $\therefore \left.\frac{m_{\mathrm{ion}}}{q_{\mathrm{ion}}}\right|_{t=1150.01} = 28.047 \approx 28$
  The corresponding ion fragment is: $C_2H_4^+$

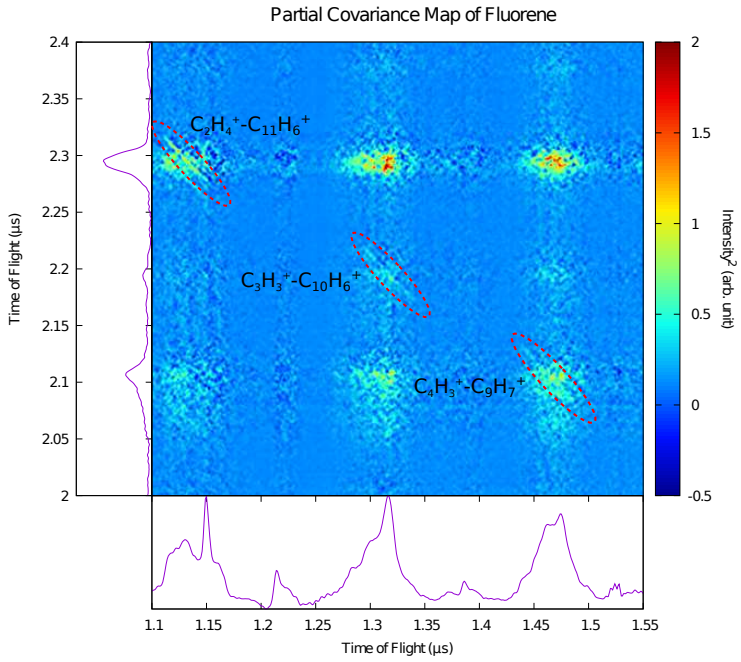


Figure 1.3.2: Partial covariance map of fluorene shows the Coulomb explosions marked with dashed ellipses. It also gives us the idea about which ion fragments are responsilbe for those Coulomb explosions and here we see the $C_2$, $C_3$, and $C_4$ losses from the parent PAH.

Time of flight of second ion: 2295.06 ms

$\therefore \left.\frac{m_{\text{ion}}}{q_{\text{ion}}}\right|_{t=2295.06} = 138.99$

The corresponding ion fragment is: $C_{11}H_6^+$

So from this we see $C_2$ loss from the parent PAH.

- **$C_3$** loss:

  Time of flight of first ion: 1316.63 ms

  $\therefore \left.\frac{m_{\text{ion}}}{q_{\text{ion}}}\right|_{t=1316.63} = 38.9 \approx 39$

  The corresponding ion fragment is: $C_3H_3^+$

  Time of flight of second ion: 2193.93 ms

  $\therefore \left.\frac{m_{\text{ion}}}{q_{\text{ion}}}\right|_{t=2193.93} = 125.80 \approx 126$

  The corresponding ion fragment is: $C_{10}H_6^+$

So from this we see $C_3$ loss from the parent PAH and also we have a loss of hydrogen in the process.

- **$C_4$** loss:

  Time of flight of first ion: 1474.46 ms

  $\therefore \left.\frac{m_{\text{ion}}}{q_{\text{ion}}}\right|_{t=1474.46} = 50.92 \approx 51$

  The corresponding ion fragment is: $C_4H_3^+$

  Time of flight of second ion: 2107.03 ms

  $\therefore \left.\frac{m_{\text{ion}}}{q_{\text{ion}}}\right|_{t=2107.03} = 114.99 \approx 115$

  The corresponding ion fragment is: $C_9H_7^+$

  So from this we see $C_4$ loss from the parent PAH.

#### 1.3.2.2 Phenanthrene

Molecular formula of phenanthrene: $C_{14}H_{10}$

Molar mass of phenanthrene: 178 g/mol

2D structure of phenanthrene:

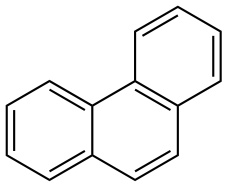

**Calibration for phenanthrene:**

From the TOF Mass spectrum of phenanthrene in Fig. 1.3.1, We have,

$$\frac{m_{\text{Phen}^+}}{q_{\text{Phen}^+}} = 178,\ \frac{m_{\text{He}^+}}{q_{\text{He}^+}} = 4$$
$$t_{\text{Phen}^+} = 2574,\ t_{\text{He}^+} = 570$$

(Phen : Phenanthrene, He : Helium)

Plugging the values in eqn. 1.5 and solving for $K_{\text{ins}}$ and $t_0$, we finally get,

$$\boxed{K_{\text{ins}} = 3.203 \times 10^{-5}, \text{and } t_0 = 216.6127}$$

From the partial covarinace map we have plotted, shown in the Fig. 1.3.3 and 1.3.4, we see four lines corresponding to Coulomb explosions.

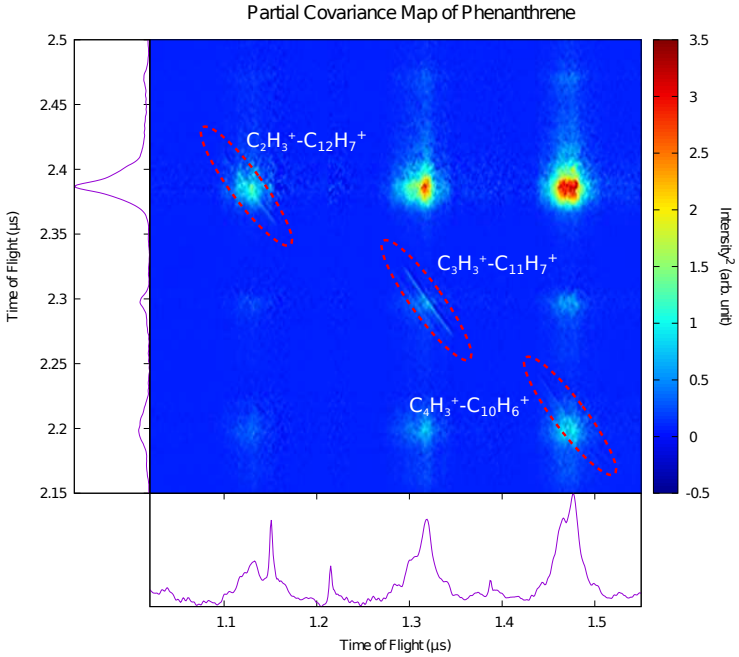


Figure 1.3.3: The graph for partial covariance map of phenanthrene showing the Coulomb explosions marked with the ellipse. It also shows the ion fragments responsible for the Coulomb explosions and here we see $C_2$, $C_3$, and $C_4$ losses from the parent PAH.

- **$C_2$** loss:

  Time of flight of first ion: 1133.01 ms

  $\therefore \left.\frac{m_{\text{ion}}}{q_{\text{ion}}}\right|_{t=1133.01} = 26.89 \approx 27$

  The corresponding ion fragment is: $C_2H_3^+$

  Time of flight of second ion: 2386.98 ms

  $\therefore \left.\frac{m_{\text{ion}}}{q_{\text{ion}}}\right|_{t=2386.98} = 150.878 \approx 151$

  The corresponding ion fragment is: $C_{12}H_7^+$

  So from this we see $C_2$ loss from the parent PAH.

- **$C_3$** loss:

  Time of flight of first ion: 1318.55 ms

  $\therefore \left.\frac{m_{\text{ion}}}{q_{\text{ion}}}\right|_{t=1318.55} = 38.91 \approx 39$

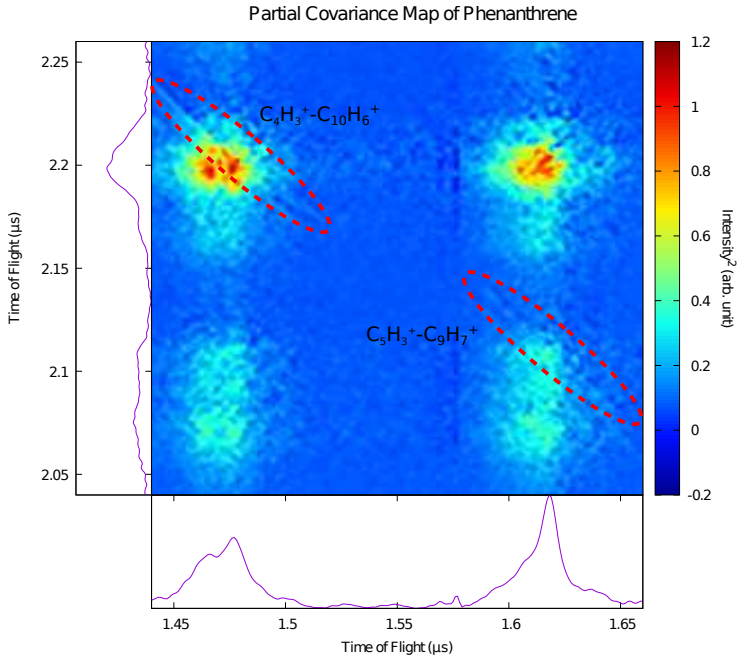


Figure 1.3.4: This shows $C_5$ loss from the parent ion and the corresponding ion fragments for the Coulomb explosion.

The corresponding ion fragment is: $C_3H_3^+$

Time of flight of second ion: 2297.17 ms

$\therefore \left.\frac{m_{\text{ion}}}{q_{\text{ion}}}\right|_{t=2297.17} = 138.649 \approx 139$

The corresponding ion fragment is: $C_{11}H_7^+$

So from this we see $C_3$ loss from the parent PAH.

- **$C_4$** loss:

  Time of flight of first ion: 1477.01 ms

  $\therefore \left.\frac{m_{\text{ion}}}{q_{\text{ion}}}\right|_{t=1477.01} = 50.88 \approx 51$

  The corresponding ion fragment is: $C_4H_3^+$

  Time of flight of second ion: 2198.69 ms

  $\therefore \left.\frac{m_{\text{ion}}}{q_{\text{ion}}}\right|_{t=2198.69} = 125.834 \approx 126$

  The corresponding ion fragment is: $C_{10}H_6^+$

So from this we see $C_4$ loss from the parent PAH and also we see a hydrogen loss in the total process.

- **$C_5$** loss:

  Time of flight of first ion: 1618.44 ms

  $\therefore \left.\frac{m_{\text{ion}}}{q_{\text{ion}}}\right|_{t=1618.44} = 62.943 \approx 63$

  The corresponding ion fragment is: $C_5H_3^+$

  Time of flight of second ion: 2108.80 ms

  $\therefore \left.\frac{m_{\text{ion}}}{q_{\text{ion}}}\right|_{t=2108.80} = 114.68 \approx 115$

  The corresponding ion fragment is: $C_9H_7^+$

  So from this we see $C_5$ loss from the parent PAH.

#### 1.3.2.3 Pyrene

Molecular formula of pyrene: $C_{16}H_{10}$

Molar mass of pyrene: 202 g/mol

2D structure of pyrene:

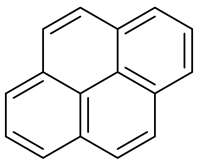

**Calibration for pyrene:**

From the TOF Mass spectra of pyrene in Fig. 1.3.1, We have,

$$\frac{m_{\text{Pyr}^+}}{q_{\text{Pyr}^+}} = 202,\ \frac{m_{\text{He}^+}}{q_{\text{He}^+}} = 4$$
$$t_{\text{Pyr}^+} = 1362,\ t_{\text{He}^+} = 284$$
$$(\text{Pyr}:\ \text{Pyrene},\ \text{He}:\ \text{Helium})$$

Plugging the values in eqn. 1.5 and solving for $K_{\text{ins}}$ and $t_0$, we finally get,

$$\boxed{K_{\text{ins}} = 12.834 \times 10^{-5}, \text{and } t_0 = 107.4620}$$

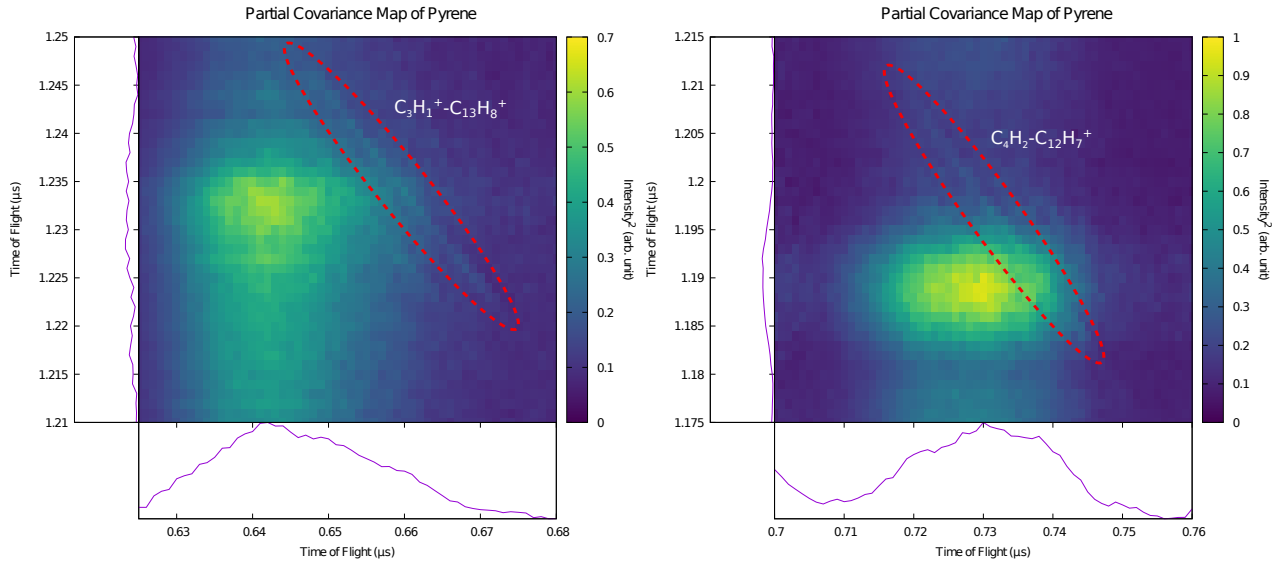


(a) (b)

Figure 1.3.5: a) $C_3$ loss and b) $C_4$ loss are observed from the partial covariance map of pyrene. In both explosions we see loss of hydrogens.

From the covarinace map we have plotted in Fig. 1.3.5a and 1.3.5b, we see only two lines corresponding to Coulomb explosions.

- **$C_3$** loss:

  Time of flight of first ion: 642.035 ms

  $\therefore \left.\frac{m_{\text{ion}}}{q_{\text{ion}}}\right|_{t=642.035} = 36.677 \approx 37$

  The corresponding ion fragment is: $C_3H_1^+$

  Time of flight of second ion: 1236.99 ms

  $\therefore \left.\frac{m_{\text{ion}}}{q_{\text{ion}}}\right|_{t=1236.99} = 163.749 \approx 164$

  The corresponding ion fragment is: $C_{13}H_8^+$

  So from this we see $C_3$ loss from the parent PAH also we have a loss of hydrogen in the process.

- **$C_4$** loss:

Time of flight of first ion: 730.51 ms

$\therefore \left.\frac{m_{\text{ion}}}{q_{\text{ion}}}\right|_{t=730.51} = 49.82 \approx 50$

The corresponding ion fragment is: $C_4H_2^+$

Time of flight of second ion: 1192.01 ms

$\therefore \left.\frac{m_{\text{ion}}}{q_{\text{ion}}}\right|_{t=1192.01} = 150.9 \approx 151$

The corresponding ion fragment is: $C_{12}H_7^+$

So from this we see $C_4$ loss from the parent PAH with a hydrogen loss from system.

### 1.3.3 Group 2

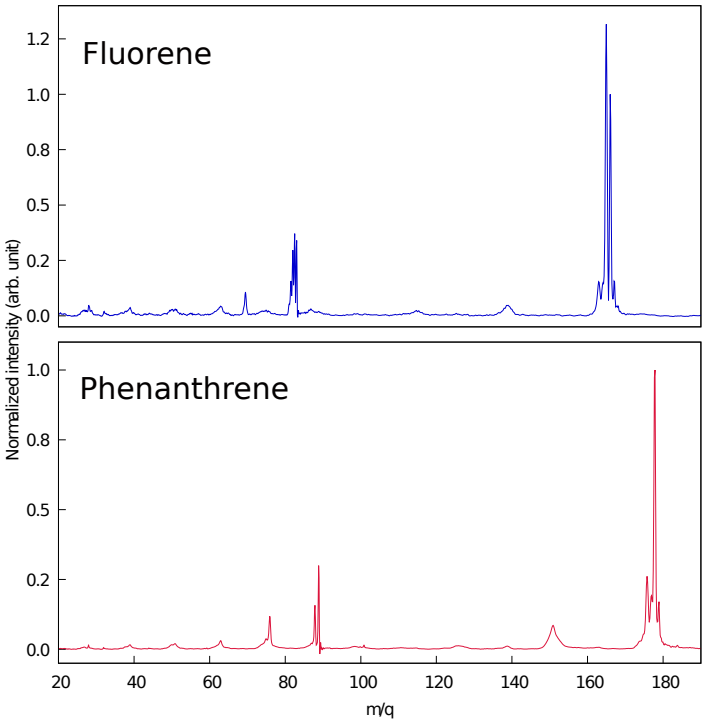


Figure 1.3.6: Time of flight Mass spectra of fluorene and phenanthrene.

The experiemntal conditions for the Group 1 are:

1. FEL pump
2. 400 nm probe.

3. Delay scan is on.

In this group we have two PAHs to work with and those are fluorene and phenathrene and the time of flight mass spectrum of ions are shown in Fig. 1.3.6. In this group we have mixture of long range and short range delay scan rather than only short range scan which was in group 1. In principle, it is a bad method of analyzing the data for long and short range delay scan but due to small amount of dataset and to check whether it affects the initial data or not, this is done.

#### 1.3.3.1 Fluorene

**Calibration for fluorene:**

From the TOF Mass spectra of fluorene in Fig. 1.3.6, We have,

$$\frac{m_{\mathrm{Flu}^+}}{q_{\mathrm{Flu}^+}} = 166,\ \frac{m_{\mathrm{He}^+}}{q_{\mathrm{He}^+}} = 4$$
$$t_{\mathrm{Flu}^+} = 2488,\ t_{\mathrm{He}^+} = 569$$
$$(\mathrm{Flu}:\ \text{Fluorene},\ \mathrm{He}:\ \text{Helium})$$

Plugging the values in eqn. 1.5 and solving for $K_{\mathrm{ins}}$ and $t_0$, we get,

$$\boxed{K_{\mathrm{ins}} = 3.2168 \times 10^{-5}, \text{and } \mathrm{t}_0 = 216.3754}$$

From the partial covariance map we have plotted in Fig. 1.3.7, we see three lines corresponding to Coulomb explosions.

- $\mathbf{C_2}$ loss:

  Time of flight of first ion: 1130.01 ms

  $\therefore \left.\frac{m_{\mathrm{ion}}}{q_{\mathrm{ion}}}\right|_{t=1130.01} = 26.85 \approx 27$

  The corresponding ion fragment is: $C_2H_3^+$

  Time of flight of second ion: 2295.57 ms

  $\therefore \left.\frac{m_{\mathrm{ion}}}{q_{\mathrm{ion}}}\right|_{t=2295.57} = 139.06 \approx 139$

  The corresponding ion fragment is: $C_{11}H_7^+$

  So from this we see $C_2$ loss from the parent PAH.

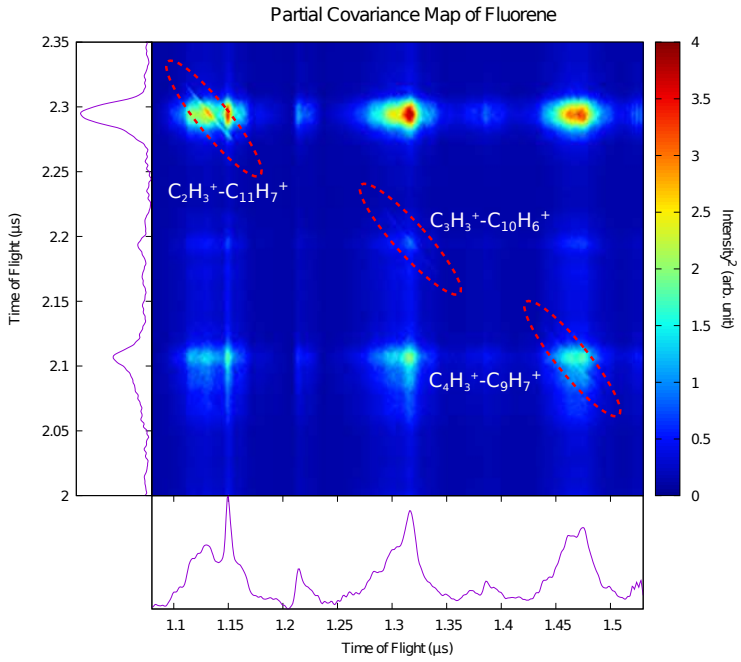


Figure 1.3.7: Partial covariance map of fluorene shows the Coulomb explosions marked with the ellipse. It also gives the idea about which ion fragments are responsilbe for those Coulomb explosions and here we see the $C_2$, $C_3$, and $C_4$ losses from the parent PAH.

- **$C_3$** loss:

  Time of flight of first ion: 1316.01 ms

  $\therefore \left.\frac{m_{\text{ion}}}{q_{\text{ion}}}\right|_{t=1316.01} = 38.89 \approx 39$

  The corresponding ion fragment is: $C_3H_3^+$

  Time of flight of second ion: 2194.01 ms

  $\therefore \left.\frac{m_{\text{ion}}}{q_{\text{ion}}}\right|_{t=2194.01} = 125.81 \approx 126$

  The corresponding ion fragment is: $C_{10}H_6^+$

  So from this we see $C_3$ loss from the parent PAH and also we have a loss of hydrogen in the process.

- **$C_4$** loss:

  Time of flight of first ion: 1475 ms

$\therefore \frac{m_{\text{ion}}}{q_{\text{ion}}}\Big|_{t=1475} = 50.96 \approx 51$

The corresponding ion fragment is: $C_4H_3^+$

Time of flight of second ion: 2107.01 ms

$\therefore \frac{m_{\text{ion}}}{q_{\text{ion}}}\Big|_{t=2107.01} = 114.99 \approx 115$

The corresponding ion fragment is: $C_9H_7^+$

So from this we see $C_4$ loss from the parent PAH.

#### 1.3.3.2 Phenanthrene

From the TOF Mass spectra of phenanthrene in Fig. 1.3.6, We have,

$$\frac{m_{\text{Phen}^+}}{q_{\text{Phen}^+}} = 178,\ \frac{m_{\text{He}^+}}{q_{\text{He}^+}} = 4$$
$$t_{\text{Phen}^+} = 2573,\ t_{\text{He}^+} = 569$$

(Phen : phenanthrene, He : Helium)

Plugging the values in eqn. 1.5 and solving for $K_{\text{ins}}$ and $t_0$, we finally get,

$$\boxed{K_{\text{ins}} = 3.203 \times 10^{-5}, \text{and } t_0 = 215.6127}$$

From the covariance we have plotted in Fig. 1.3.8 and 1.3.9, we see four lines corresponding to Coulomb explosions.

- **$C_2$** loss:

  Time of flight of first ion: 1133.01 ms

  $\therefore \frac{m_{\text{ion}}}{q_{\text{ion}}}\Big|_{t=1133.01} = 26.951 \approx 27$

  The corresponding ion fragment is: $C_2H_3^+$

  Time of flight of second ion: 2386.99 ms

  $\therefore \frac{m_{\text{ion}}}{q_{\text{ion}}}\Big|_{t=2386.99} = 151.018 \approx 151$

  The corresponding ion fragment is: $C_{12}H_7^+$

  So from this we see $C_2$ loss(Fig. 1.3.9) from the parent PAH.

- **$C_3$** loss:

  Time of flight of first ion: 1319.00 ms

  $\therefore \frac{m_{\text{ion}}}{q_{\text{ion}}}\Big|_{t=1319.00} = 38.99 \approx 39$

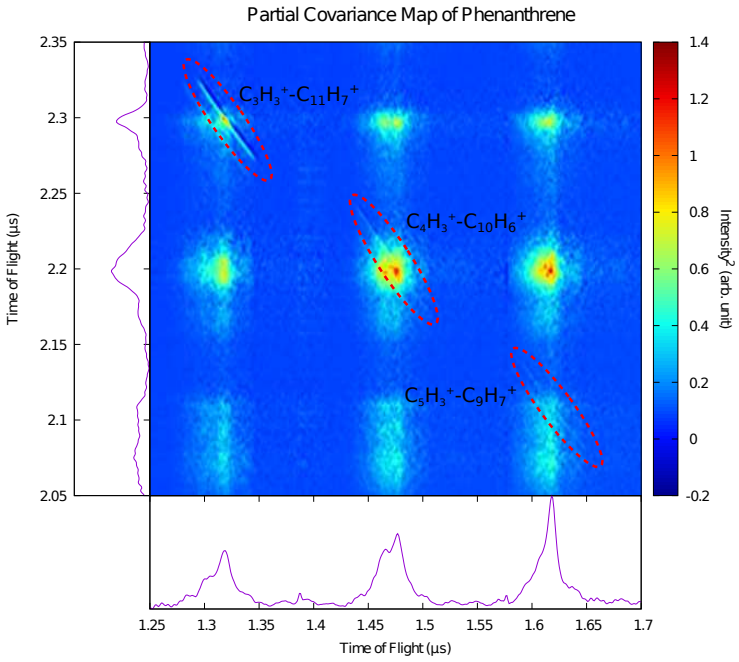


Figure 1.3.8: Partial covariance map of phenanthrene showing the Coulomb explosions marked with the ellipse. It also shows the ion fragments responsible for the Coulomb explosions and here we see the $C_3$, $C_4$, and $C_5$ losses from the parent PAH.

The corresponding ion fragment is: $C_3H_3^+$

Time of flight of second ion: 2298.01 ms

$\therefore \left.\frac{m_{\text{ion}}}{q_{\text{ion}}}\right|_{t=2298.01} = 138.895 \approx 139$

The corresponding ion fragment is: $C_{11}H_7^+$

So from this we see $C_3$ loss from the parent PAH.

- **$C_4$** loss:

  Time of flight of first ion: 1477.01 ms

  $\therefore \left.\frac{m_{\text{ion}}}{q_{\text{ion}}}\right|_{t=1477.01} = 50.96 \approx 51$

  The corresponding ion fragment is: $C_4H_3^+$

  Time of flight of second ion: 2199.01 ms

  $\therefore \left.\frac{m_{\text{ion}}}{q_{\text{ion}}}\right|_{t=2199.01} = 126.001 \approx 126$

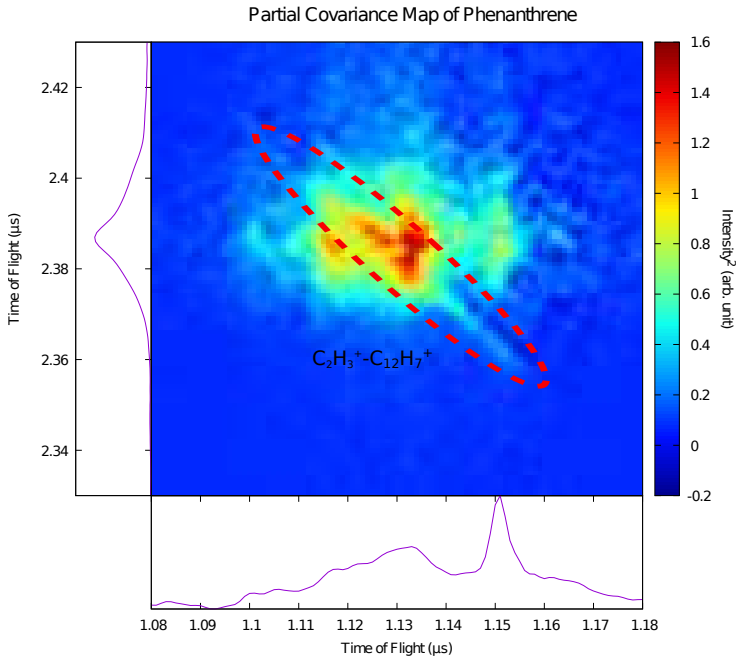


Figure 1.3.9: This partial covariance of phenanthrene shows the $C_2$ loss from the parent ion and the corresponding ion fragments for the Coulomb explosion.

The corresponding ion fragment is: $C_{10}H_6^+$

So from this we see $C_4$ loss from the parent PAH and also we see a hydrogen loss in the total process.

- **$C_5$** loss:

  Time of flight of first ion: 1618.02 ms

  $\therefore \left.\frac{m_{\text{ion}}}{q_{\text{ion}}}\right|_{t=1618.02} = 62.995 \approx 63$

  The corresponding ion fragment is: $C_5H_3^+$

  Time of flight of second ion: 2108.01 ms

  $\therefore \left.\frac{m_{\text{ion}}}{q_{\text{ion}}}\right|_{t=2108.01} = 114.71 \approx 115$

  The corresponding ion fragment is: $C_9H_7^+$

  So from this we see $C_5$ loss from the parent PAH.

## 1.4 Conclusion

The main objective of this part of the project was to find the Coluombic explosions from the partial covariance map of photoion-photoion correlation and to find the responsible frgament channels corresponding to those explosions. And it was a good success as we have seen many of those explosions for three different molecules. We found the Coulomb explosions and the fragment channels for the same. In the case of phenanthrene we see four channels responsible for Coulomb explosions and the channels are $C_2$, $C_3$, $C_4$ and $C_5$ losses from parent ion. In fluorene the signal to noise ratio is quite low, but we were able to find the channels for $C_2$, $C_3$ and $C_4$ losses. We have found only two channels, $C_3$ and $C_4$ losses fcorresponding to Coulomb explosions in case of pyrene. Most importantly when we have analazyed the Group 2 of mixed delay scans, we see that the channels responsible for Coulomb explosions the position in the TOF mass spectra are same as that of before.

# Chapter 2

# Theoretical Simulation of Pump-probe Dynamics in Naphthalene

# Introduction

With the development of ultrfast chemistry, pump-probe studies have been very useful for understanding and analyzing the reaction mechanisms, tracing the transition states and short-lived species. The mechanism of such studies is as follows. At first a laser pulse, which is termed as pump pulse, is given to the target molecule and it excites the molecular dynamics. After that a second laser pulse which is delayed with respect to the pump pulse is given to the molecule and it scans the transient dyanamics of the molecule. It is not always that the pump pulse will come before the probe pulse. The probe pulse is either positively delayed or negatively delayed w.r.t the pump pulse. The positive delay is that the pump pulse comes probe pulse and the negative delay means that the probe pulse comes before the pump pulse. Based on the pump, probes and outcoming signal we perform pump-probe ion-electron spectroscopy[11]. One of the possible signals are the yields of the electrons and ion fragments of the initial molecule, that are usually registered using VMI technique. Our main point of interest is the simulation of fragmentation dynamics, i.e. the yields of different fragments under different pump-probe delays. Among the simulations of pump-probe dynamics and processes behind it, the most prominent and theoretically justified are the time-dependent nuclear quantum dynamics, such as MCTDH (multiconfiguration time-dependent Hartree method) and AIMS (*ab initio* multiple spawning), that allows to look into the behavior of wavepackets on multiple electronic surfaces. Unfortunately these methods of modelling are very time consuming and can be applied only to small systems. If we neglect the quantum nature of nuclei then we can have cheaper simulations for the the classical trajectories which is known as molecular dynamics (MD). As we are focusing on the pump-probe dynamics with the involvement of electronic transition, we take into account motions in multiple electronic states and so this types of simulations employ a sort of non-adiabatic MD, trajectory surface hopping dynamics (TSHD)[1, 5, 10]. However, the TSHD is much more expensive then the regular MD on the ground electronic surface, namely Born-Oppenheimer MD (BOMD). A recent methodology was proposed for theoretical prediction of electron impact mass spectra (EIMS) based on the BOMD, which is called QCEIMS[6, 13]. In this work we have tried to apply the simplified methodology to the pump-probe fragmentation dynamics employing

XUV photons as a pump pulse. We assume that the molecule $A$ undergoes the reaction $A + h\nu_{\mathrm{XUV}} \rightarrow (A^{n+})^* + ne^-$, where $(A^{n+})^*$ denotes excited electronic state of $n$-cation of $A$. The probe pulse, which is either positively or negatively delayed, introduces some additional electronic excitations to the state of the molecule. This leads to the energy transfer from electronic excitation to the vibrational degrees freedom which actually helps in in the process of fragmentation and can be traced down by BOMD.

## 2.1 Introduction to general structure of simulations

The root of the simulation of mass-spectra in pump-probe spectroscopy is lied in the EIMS simulations within QCEIMS method. However, in case of pump-probe spectra the molecule is subjected to two excitations instead of one. We have used the following algorithm for

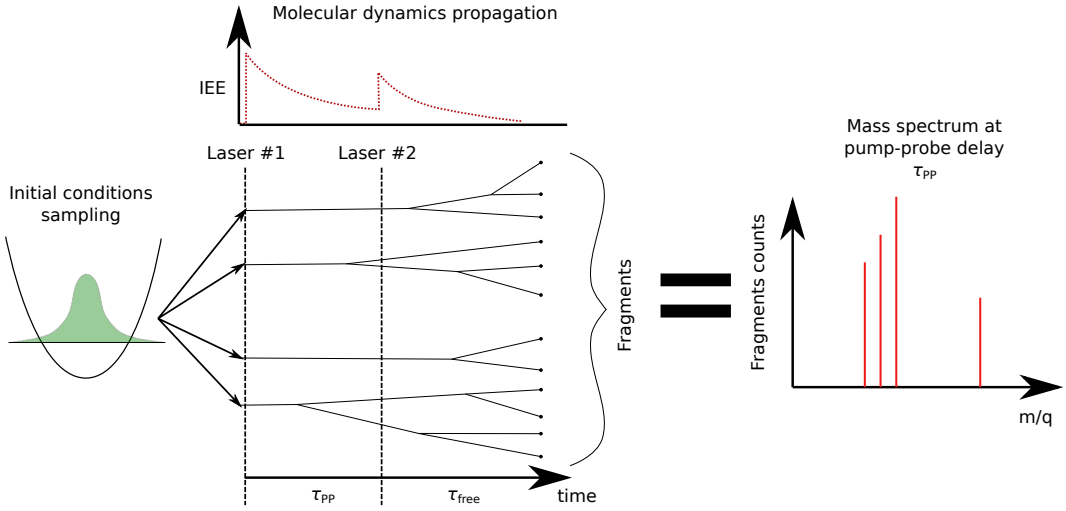


Figure 2.1.1: A schematic representation of molecular dynamics simulation of fragmentation signals for ultrafast pump-probe spectroscopy.

modelling:

- Generation of initial structures. This can be done in the same way as in the QCEIMS[13]. We have generated initial conditions from Wigner distribution obtained from harmonic oscillator approximation of molecule at equilibrium geometry. The generation was performed using scripts from DFTBaby package based on the GFN2-xTB force field. The

obtained ensemble of initial conditions represent the molecule at $T = 0$ K. However, since the energies of ground level motions $E = h\nu/2$, where $\nu$ is the frequency of the vibration, for most of the molecular vibrations are above the usual temperatures of experiment $T \approx 300 - 500$ K ($\nu$ of 200 – 350 cm$^{-1}$), the obtained initial conditions will represent molecules better, than the ones obtained from Maxwell-Boltzmann distributions.

- We then performed the Born-Oppenheimer molecular dynamics (BOMD) simulation for the chosen ensemble of initial conditions. The overall time of simulation for each inital condition is $\tau_{\mathrm{PP}} + \tau_{\mathrm{free}}$, where $\tau_{\mathrm{PP}}$ is the pump-probe delay and the $\tau_{\mathrm{free}}$ is a free time for molecule to fragment, around 2-3 ps in the calculations we have done. The electronic excitation is modelled via additional degree of freedom, namely internal excess energy (IEE)(as introduced in QCEIMS). The energy from this degree of freedom is constantly drained into the intramolecular vibrations via first order dynamics equation, $\frac{d\mathrm{IEE}}{dt} = -k_{\mathrm{IC}}\mathrm{IEE}$, where $k_{\mathrm{IC}}$ is an internal conversion constant representing electronic excitation decay via nonadiabatic processes (e.g. passing of conical intersections and avoided crossings etc.).

- The in-charge-state electronic excitations can be emulated as an increase on IEE by pre-set value or as a change in electronic state multiplicity. The ionization by laser, in addition to previous changes, increase the charge state of the molecule. The first laser comes at the first step of the simulation, and the second acts after time of $\tau_{\mathrm{PP}}$ has passed.

- During the molecular dynamics simulations occurances of possible molecular fragmentations are detected based on the analysis of molecular graph constructed from interatomic distances by a standard criterion of bonds which is $r_{ij} \leq s \cdot (R_i + R_j)$, where $r_{ij}$ is the interatomic distance between atoms $i$ and $j$, $R$ is the atomic radius and $s$ is a scale factor in between 1 and 2 (we have taken 1.5)[2]. If the fragmentation of molecule $M^{n+}$ with charge into two fragments $A^{a+}$ and $B^{b+}$ are detected, a calculation of all possible dissociation energies for reactions $M^{n+} \rightarrow A^{a+} + B^{b+}$ with $a + b = n$ and $a, b \geq 0$ are performed. If the kinetic energy of center of masses of these fragments is

greater than the dissociation energy, then they overcome the mutual interaction and they get seperated. After dissociation simulation of $M^{n+}$ stops and at that very moment the molecular dynamics simulations of the fragments $A^{a+}$ and $B^{b+}$ get initiated with the lowest dissociation threshold. The IEE of $M^{n+}$ is splitted proportionally to the number of electrons in the fragments $A^{a+}$ and $B^{b+}$: $\mathrm{IEE}(C) = \mathrm{IEE}(M^{n+})\frac{N_\mathrm{e}(C)}{N_\mathrm{e}(M^{n+})}$, $C = A^{a+}, B^{b+}$ and $N_\mathrm{e}$ is the number of electrons.

- After the simulations are over, we then calculated the mass spectrum from the fragment channels detected over the simulation for particular pump-probe delay $\tau_\mathrm{PP}$ between the lasers.

For each desired pump-probe delay the mass spectrum $I_\mathrm{MS}(m/q, \tau_\mathrm{PP})$ should be obtained, which makes the simulation of fragmentation dynamics to be more costly, than the regular EIMS prediction. To obtain a better consistency with the experimental data, the calculated fragmentation yields $I_\mathrm{MS}(m/q, \tau_{PP})$ can be convoluted with the instrumental function of $\exp\left(-\frac{t^2}{\tau_\mathrm{cc}^2}\right)$, where $\tau_\mathrm{cc}$ is the cross-correlation time consisting of the laser pulses widths.

### 2.1.1 Internal excess energy and Internal conversion rate

The QCEIMS assigns IEE using the Poisson-type distribution with two adjustable parameters. We have derived an over-simplified analytical model to estimate IEE after ionization. Let us take an example to explain. By considering a molecule M and the conventional way for ionization we see $\mathrm{M}^{(0)}$ + ionizing radiation $\rightarrow \mathrm{M}^{(\mathrm{q}+)} + q\mathrm{e}^-$ which is shown in Fig. 2.1.2. The internal excess energy is the energy difference between electronic energy of the final state of $\mathrm{M}^{(\mathrm{q}+)}$ and its ground state. Let us assume that the particle of ionizing radiation has an energy of $E_\mathrm{r}$, which is equal to $E_\mathrm{r} = mh\nu$ in the case of ionization by $m$ photons with frequency $\nu$ and to $E_\mathrm{r} = \frac{m_\mathrm{e}v^2}{2}$ in case of electronic impact ionization ($m_\mathrm{e}$ is the mass of the electron and $v$ is its velocity). The energy of the ionizing particle is converted into the overcoming of the ionization potential $\mathrm{IP_q}$, IEE of the molecule in the $i$-th electronic excited state of the $\mathrm{M}^{(\mathrm{q}+)}$ ($\mathrm{IEE}_i$) and the kinetic energy of the leaving electrons ($\mathrm{T_e}$), therefore due to energy conservation law we can write

$$E_\mathrm{r} = \mathrm{IP}_q + \mathrm{IEE}_i + \mathrm{T}_{\mathrm{e},i} \ . \tag{2.1}$$

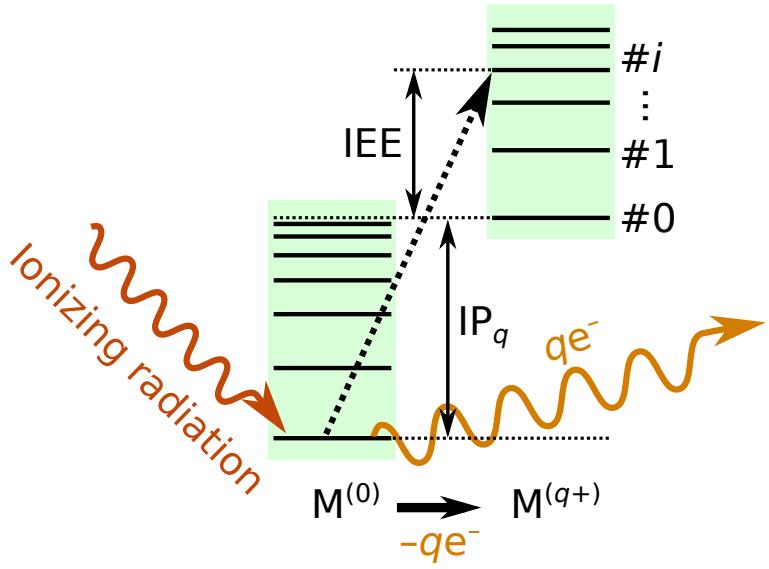


Figure 2.1.2: Jablonski diagram of the ionization of neutral molecule $\mathrm{M}^{(0)}$ by radiation via removal on $N$ electrons.

Let us assume that if this is not resonant excitation, then the system can end up in the any of the excited states ($i > 0$) as well as in the ground state ($i = 0$, $\mathrm{IEE}_0 = 0$) with equal probability. Therefore we can find a distribution of the excited states of the molecule by applying the maximum entropy principle, as it is done in kinetic modeling of the MS. The first contribution to entropy is the entropy of the ion $\mathrm{M}^{(\mathrm{q}+)}$ $S(\mathrm{M}^{(\mathrm{q}+)}) = k_\mathrm{B} \ln\left(\frac{n!}{n_0! \cdot n_1! \cdot \ldots n_i! \cdot \ldots}\right) \approx k_\mathrm{B} n \ln(n) - k_\mathrm{B} n - (\sum_i k_\mathrm{B} n_i \ln(n_i) - \sum_i k_\mathrm{B} n_i)$, where $n = n_0 + n_1 + \ldots + n_i + \ldots$ is the total number of ionized molecules, and $n_i$ is the number of ions in the $i$-th electronic state and $k_\mathrm{B}$ is the Boltzmann constant. The second contribution to entropy comes from the leaving electrons ($S_\mathrm{e}$). Number of states for the gas with $N_\mathrm{f}$ degrees of freedom in the vicinity of energy $\mathrm{T_e}$ is proportional to $\mathrm{T_e}^{\frac{N_\mathrm{f}}{2}-1}$, therefore we can estimate the $S_\mathrm{e}$ for the system as

$$S_\mathrm{e} \approx \sum_i n_i \cdot k_\mathrm{b}(\frac{N_\mathrm{f}}{2} - 1) \ln(\mathrm{T}_{\mathrm{e},i}) \ .$$

Maximization of the overall entropy with additional condition $n = \sum_i n_i$,

$$S_\mathrm{mol} + S_\mathrm{e} + \lambda(n - \sum_i n_i) \to \max$$

results in the distribution of the molecules in the excited state $n_i \propto (\mathrm{T}_{\mathrm{e},i})^{(\frac{N_\mathrm{f}}{2}-1)}$, which after application of Eq. 2.1 is transformed into:

$$n_i \propto (E_\mathrm{r} - \mathrm{IP}_q - \mathrm{IEE}_i)^{(\frac{N_\mathrm{f}}{2}-1)} \ . \tag{2.2}$$

Obviously, the requirements $E_\mathrm{r} \geq \mathrm{IP}_q + \mathrm{IEE}_i$ and $\mathrm{IEE}_i$ being smaller than ionization potential of $\mathrm{M}^{(\mathrm{q}+)}$ should be fulfilled for application of this distribution. The $N_\mathrm{f}$ of the electrons is equal to $3q$ in case of photoionization, and to $3(q+1)$ in case of EI, because the ionizing electron also leaves the molecule. As it can be seen, this distribution to in contrast to one in the QCEIMS does not have any free parameters, and makes a clear physical sense. The only thing that it requires are the energies of the excited states of the ion $\mathrm{M}^{(\mathrm{q}+)}$.

We have used the other model for the internal conversion rates comparing to one implemented in QCEIMS.[13] Let us do a simple calculation to visualize the inter conversion rate. Imagine the internal conversion as a hot electric gas heating cold nuclei. We will consider a simplest model of two colliding classical particles: one of them (electron) has a mass of $m_\mathrm{e}$ and energy $\frac{m_\mathrm{e}v_0^2}{2} = \mathrm{IEE}/3$, the second one (nucleus) has a mass $M$ and does not move before the collision. We will assume collusion an elastic one, therefore after application of energy and momentum conservation laws we will obtain velocity of the electron after the collision to be $v_1 = v_0 \cdot \frac{m_\mathrm{e}-M}{m_\mathrm{e}+M}$. Thus the kinetic energy loss of the electron is $\delta T = \frac{m_\mathrm{e}v_1^2}{2} - \frac{m_\mathrm{e}v_0^2}{2} = -\underbrace{\frac{m_\mathrm{e}v_0^2}{2}}_{\mathrm{IEE}/3} \cdot \frac{4m_\mathrm{e}M}{(m_\mathrm{e}+M)^2} \approx \frac{4}{3}\frac{m_\mathrm{e}}{M}\mathrm{IEE}$. If the molecule contains $N_\mathrm{n}$ nuclei with masses $M_1, M_2, \ldots, M_n$, and the electrons collide with $i$-th nuclei with frequency $\nu_i$, the decay of the IEE can be described with a first-order ordinary differential equation:

$$\frac{d}{dt}\mathrm{IEE} = -\underbrace{\left(\sum_i \overbrace{\frac{4}{3}\nu_i\frac{m_\mathrm{e}}{M_i}}^{k_{\mathrm{IC},i}}\right)}_{k_\mathrm{IC}} \mathrm{IEE} = -k_\mathrm{IC} \cdot \mathrm{IEE} \ , \tag{2.3}$$

where $k_\mathrm{IC}$ is the internal conversion rate. A good approximation for the collision frequency of electrons with nucleus seems to be the so-called electron plasma (or Langmuir) frequency:

$$\nu_i = 2\pi\sqrt{n_{\mathrm{e},i}\frac{q_\mathrm{e}^2}{\varepsilon_0 m_\mathrm{e}}} \ ,$$

where $n_{e,i}$ is the electron density on the $i$-th nucleus, $q_e$ is the charge of electron, and $\varepsilon_0$ is the vacuum permittivity. The simplest on-the-fly estimation of electron density is the following:

$$n_{e,i} \approx \frac{N_{at,i}}{V_{at,i}} \approx \frac{3N_{at,i}}{4\pi R^3_{VdW,i}} \ ,$$

where $N_{at,i} = Z_i - Q_{at,i}$ is the number of electrons on the $i$-th atom, $Z_i$ is the nucleus charge and $Q_{at,i}$ is the atomic charge computed by any charge partition scheme (Mulliken, Löwdin, Hirschfeld, etc.), $V_{at,i}$ is the volume of the $i$-th atom estimated as the volume of sphere with radius equal to Van der Waals radius for $i$-th atom.

Following the solution of equation 2.3 we can evaluate the value of IEE on the next time step $\mathrm{IEE}(t + \Delta t) = \mathrm{IEE}(t)\exp(-k_{IC}\Delta t)$, thus the energy difference of $\Delta_{\Delta t}\mathrm{IEE} = \mathrm{IEE}(t) - \mathrm{IEE}(t + \Delta t) = \mathrm{IEE}(t)(1 - \exp(-k_{IC}\Delta t))$ is assigned to nuclei. In the simplest case it can be done with standard uniform velocity rescaling. However, this energy can be redistributed between atoms unequally, by adding to each atom's velocity a random vector that would increase the total kinetic energy of the system on the value $\frac{k_{IC,i}}{k_{IC}} \cdot \Delta_{\Delta t}\mathrm{IEE}$.

## 2.2 Calculation details

The simulations were performed using home-written molecular dynamics code[1] in Python, using XTB software as a source of potential energy surfaces at GFN2-xTB level of theory. The ionization potentials and excited states levels were calculated at DFT/TD-DFT levels using Orca 4 program suit at PBE0/def2-TZVPP level of theory with RI approximation utilizing def2-TZVP/C auxiliary basis sets. The molecular geometry was pre-optimized at the ground charge state, followed by single point energy calculation and TD-DFT excited states calculation of different charge states at the frozen geometry. The initial ensemble of trajectories was calculated using Python script from DFTBaby package. All the calculations have been performed on Maxwell supercomputer at DESY.

[1] Code written by Dr. Denis Tikhonov, FS-SMP, Deutsches Elektronen Synchrotron (DESY), Nottkestraße 85, 22607 Hamburg, Germany

## 2.3 Testing of the simulation method with napthalene

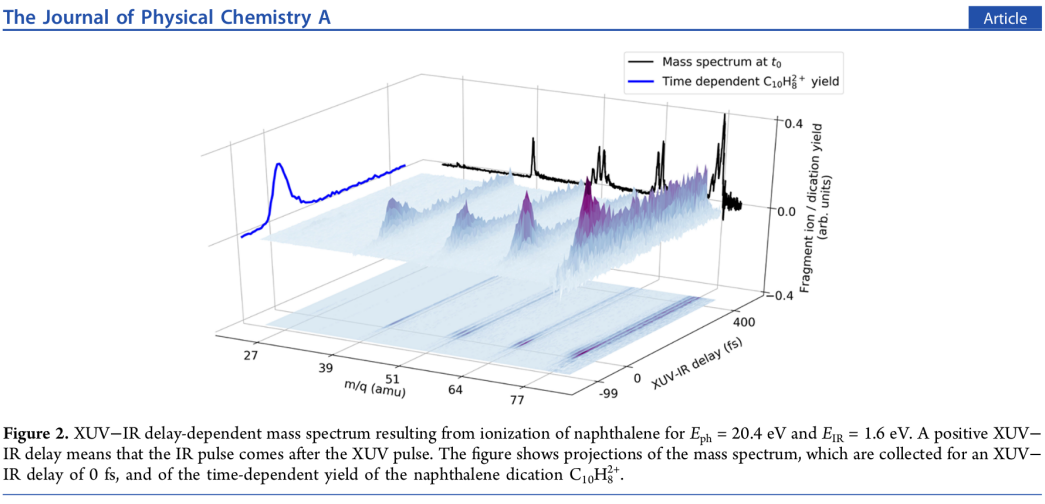


**Figure 2.** XUV−IR delay-dependent mass spectrum resulting from ionization of naphthalene for $E_{ph}$ = 20.4 eV and $E_{IR}$ = 1.6 eV. A positive XUV−IR delay means that the IR pulse comes after the XUV pulse. The figure shows projections of the mass spectrum, which are collected for an XUV−IR delay of 0 fs, and of the time-dependent yield of the naphthalene dication $C_{10}H_8^{2+}$.

Figure 2.3.1: The figure is copied from the experimental findings in the paper of Reitsma et al. [9].

We have tried to reproduce the experimental study by Reitsma et al. [9]. They have used two-color pump probe experiment made using XUV pump pulse with photon energies of 20.4, 23.6, 26.7, and 29.8 eV, generated using HHG source, and the IR probe pulse of 800 nm. So we have assumed the XUV energy to be the lowest (20.4 eV), which led to the addend to IEE from XUV pulse to be 8.7 eV computed using formula 2.2. Excitation of the electronic system with short pulse of IR laser happens in the multiphotonic regime, and we do not have a proper model to simulate that. Therefore we assumed, that IR pulse shuffles the populations of the chosen cationic state of molecule to be uniformly distributed over the electronic states manifold, leading to estimation of IR energy to be an average of all the electronic states energies computed with TDDFT. In case of neutral naphtalene the energy was found to be 6.5 eV, and for the cation it was 10.9 eV. The first energy was added to IEE before $t_0$, while the second corresponded to excitation of cation after the XUV ionization, thus it was assigned for $t > t_0$.

The resulting ion yields are shown in Fig. 2.3.2a and they match quite well with the pump-probe yields from the experimental data. The theoritical mass spectra is shown in Fig.

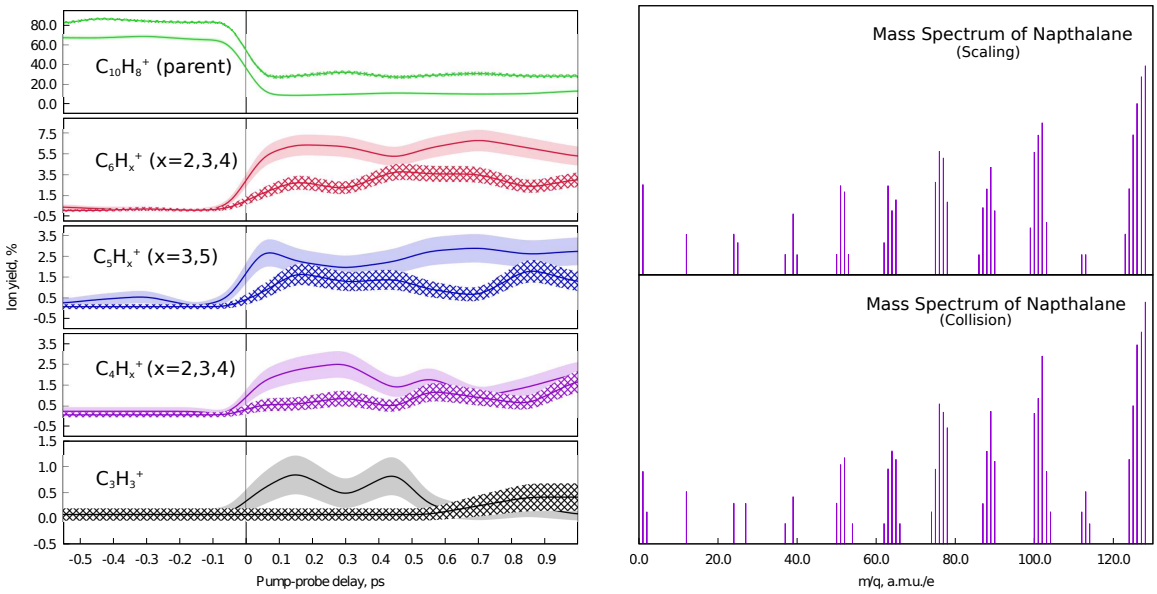


(a) (b)

Figure 2.3.2: a)Calculated pump-probe yields for naphthalene from BOMD simulations obtained in this work. The curves were convoluted with Gaussian with $\tau_{cc} = 40$ fs, that corresponds to experimenal resolution in Reitsma et al. [9]. b) Theoretical mass spectrum of napthalene averaged over all pump-probe delays. Two mass spectra correspond to the kinetic energy increase by scaling and collision for the same molecule.

2.3.2b. It is also compared that how the fragments' yields will be for two types of kinetic energy addition, one by scaling and other by collision.The largest deviations is for the lowest fragment in intensity: $C_3H_3^+$, however, this may be a result of statistical fluctuations. All the fragments show something like a transient feature for $t > t_0$. However, its value is smaller for the ones in the experiment. This inconsistency is probably due to absence of the other possible channels in the simulations, for example, ionization of the excited states of the cation with the probe photons ($C_{10}H_8^{+,*} + nh\nu_{IR} \rightarrow C_{10}H_8^{2+,*} + e^-$, see Ref. Marciniak et al. [8] for an example).

## 2.4 Conclusion

We observe a good resemblance of the result from the simulation with the experimental data. But there are a few things that can be improved.

- The IEE leftover after the ionization is a single fixed number in thesimulation, although it is a wide distribution of energies. Incorporation of that in the simulations, similar to that done in QCEIMS[13] could improve the ratios between fragmentation channels in the simulations.

- The amount of the pump or, probe addends to IEE at this point of time is computed externally at the very beginning using single point energy calculations for particular molecule of interest and therefore it would be more physically relevant, if these values could be estimated on-the-fly during BOMD simulations.

# Summary

The goal of the work presented in this report was to investigate the photofragmentation mechanisms of PAHs through both experimental and theoretical methods. To be more precise, we have investigated the PAHs exposing under XUV radiation.

We have investigated the fragmentation pathways of three PAHs (fluorene, phenanthrene and pyrene) exposed to XUV radiation using the covariance maps technique. The experiemental analysis turned out to be a sort of big data analysis of March 2018 Beamtime data at FLASH, that required learning processing of the special data storage format (HDF5), effective numerical computing using Python, and also working on the supercomputer (Maxwell @ DESY). In this work I have found the $C_2$, $C_3$ and $C_4$ fragments loss for fluorene, $C_2$, $C_3$, $C_4$ and $C_5$ fragments loss for phenanthrene and $C_3$ and $C_4$ fragments loss for pyrene.

Apart from the experimental part discussed above, we have also tried to simulate the pump-probe dynamics process to have a better understanding of the entire process. So basically we have modelled the whole process and taken a published experipental data to compare the results from the simulation with experimental one. During this work I have learned the basics of quantum chemical calculations using Orca and XTB softwares and the molecular dynamics technique. I have improved my programming skills by writing and correcting scripts in Bash and Python.

In short I must mention what I have learned during my summer project apart from theoretical knowledge. From analyzing huge chunks of data to molecular dynamics, I have aquired more skills in Python. I have learned Orca, Unex, Bash and XTB softwares. And also I have increased my skills in usage of Linux, queuening systems on clusters (SLURM), and other science-related software, such as Gnuplot.

# Bibliography


[1] Mario Barbatti. Nonadiabatic dynamics with trajectory surface hopping method. *Wiley Interdisciplinary Reviews: Computational Molecular Science*, 1(4):620–633. doi: 10.1002/wcms.64. URL https://onlinelibrary.wiley.com/doi/abs/10.1002/wcms.64.

[2] E. Clementi, D. L. Raimondi, and W. P. Reinhardt. Atomic screening constants from scf functions. ii. atoms with 37 to 86 electrons. *The Journal of Chemical Physics*, 47(4):1300–1307, 1967. doi: 10.1063/1.1712084. URL https://doi.org/10.1063/1.1712084.

[3] Leszek J Frasinski. Covariance mapping techniques. *Journal of Physics B: Atomic, Molecular and Optical Physics*, 49(15):152004, jul 2016. doi: 10.1088/0953-4075/49/15/152004. URL https://doi.org/10.1088%2F0953-4075%2F49%2F15%2F152004.

[4] LJ Frasinski, K Codling, and PA Hatherly. Covariance mapping: A correlation method applied to multiphoton multiple ionization. *Science*, 246(4933):1029–1031, 1989. doi: 10.1126/science.246.4933.1029. URL https://doi.org/10.1126/science.246.4933.1029.

[5] Murali Krishna Ganesa Subramanian, Robin Santra, and Ralph Welsch. Infrared-laser-pulse-enhanced ultrafast fragmentation of $N_2^{2+}$ following auger decay: Mixed quantum-classical simulations. *Phys. Rev. A*, 98:063421, Dec 2018. doi: 10.1103/PhysRevA.98.063421. URL https://link.aps.org/doi/10.1103/PhysRevA.98.063421.

[6] Stefan Grimme. Towards first principles calculation of electron impact mass spectra of molecules. *Angewandte Chemie International Edition*, 52(24):6306–6312. doi: 10.1002/

anie.201300158. URL https://onlinelibrary.wiley.com/doi/abs/10.1002/anie.201300158.

[7] DA Hagan and JHD Eland. Formation and decay of doubly charged ions from polycyclic aromatic hydrocarbons and related compounds. *Rapid communications in mass spectrometry*, 5(11):512–517, 1991. doi: 10.1063/1.459170. URL https://doi.org/10.1002/rcm.1290051106.

[8] A. Marciniak, V. Despré, T. Barillot, A. Rouzée, M. C. E. Galbraith, J. Klei, C.-H. Yang, C. T. L. Smeenk, V. Loriot, S. Nagaprasad Reddy, A. G. G. M. Tielens, S. Mahapatra, A. I. Kuleff, M. J. J. Vrakking, and F. Lépine. Xuv excitation followed by ultrafast non-adiabatic relaxation in pah molecules as a femto-astrochemistry experiment. *Nature Communications*, 6:7909 EP –, Aug 2015. URL https://doi.org/10.1038/ncomms8909. Article.

[9] Geert Reitsma, Johan Hummert, Judith Dura, Vincent Loriot, Marc J. J. Vrakking, Franck Lépine, and Oleg Kornilov. Delayed relaxation of highly excited cationic states in naphthalene. *The Journal of Physical Chemistry A*, 123(14):3068–3073, 2019. doi: 10.1021/acs.jpca.8b10444. URL https://doi.org/10.1021/acs.jpca.8b10444. PMID: 30888820.

[10] John C. Tully. Molecular dynamics with electronic transitions. *The Journal of Chemical Physics*, 93(2):1061–1071, 1990. doi: 10.1063/1.459170. URL https://doi.org/10.1063/1.459170.

[11] Ahmed H. Zewail. Laser femtochemistry. *Science*, 242(4886):1645–1653, 1988. ISSN 0036-8075. doi: 10.1126/science.242.4886.1645. URL https://science.sciencemag.org/content/242/4886/1645.

[12] Vitali Zhaunerchyk, LJ Frasinski, John HD Eland, and Raimund Feifel. Theory and simulations of covariance mapping in multiple dimensions for data analysis in high-event-rate experiments. *Physical Review A*, 89(5):053418, 2014. doi: 10.1103/PhysRevA.89.053418. URL https://doi.org/10.1103/PhysRevA.89.053418.

[13] Vilhjálmur Ásgeirsson, Christoph A. Bauer, and Stefan Grimme. Quantum chemical calculation of electron ionization mass spectra for general organic and inorganic molecules. *Chem. Sci.*, 8:4879–4895, 2017. doi: 10.1039/C7SC00601B. URL `http://dx.doi.org/10.1039/C7SC00601B`.

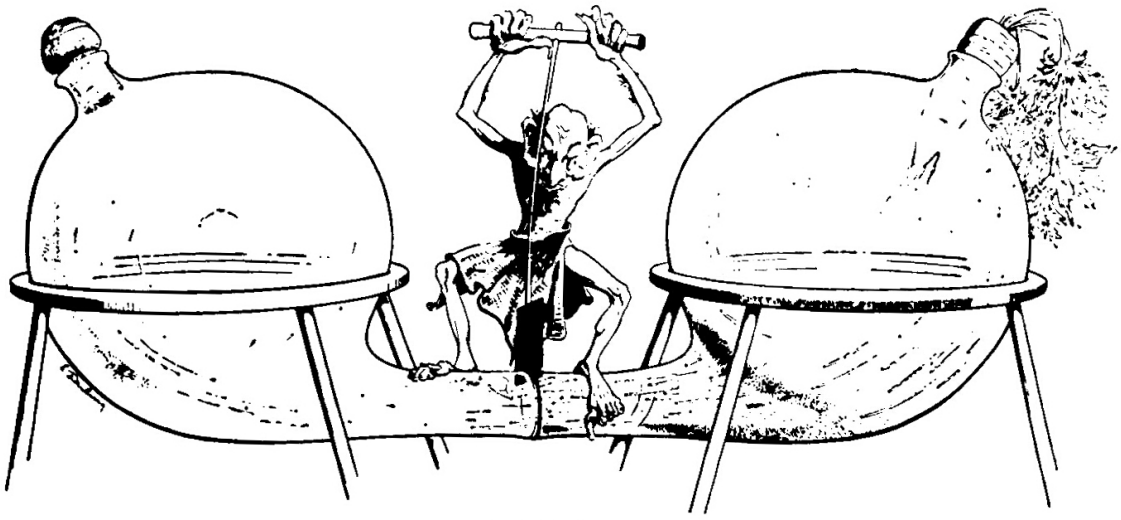

Maxwell's demon at work